JAERI 1161

JAERI 1161

# Oxidation Kinetics and Oxide Film Break-away of Zirconium and Its Alloys at High Temperatures

June 1968

日本原子力研究所

Japan Atomic Energy Research Institute

日本原子力研究所は，研究成果，調査結果の報告のため，つぎの3種の研究報告書を，それぞれの通しナンバーを付して，不定期に公刊しております．

| | | |
|---|---|---|
| 1. 研究報告 | まとまった研究の成果あるいはその一部における重要な結果の報告 | JAERI 1001-3999 |
| 2. 調査報告 | 総説，展望，紹介などを含め，研究の成果，調査の結果をまとめたもの | JAERI 4001-5999 |
| 3. 資　　料 | 研究成果の普及，開発状況の紹介，施設共同利用の手引など | JAERI 6001-6999 |

このうち既刊分については「JAERI レポート一覧」にタイトル・要旨をまとめて掲載し，また新刊レポートは「原研びぶりお」でその都度紹介しています．これらの研究報告書に関する頒布，版権，複写のお問合せは，日本原子力研究所技術情報部（茨城県那珂郡東海村）あてお申し越しください．

---

Japan Atomic Energy Research Institute publishes the nonperiodical reports with the following classfication numbers:

1. **JAERI** 1001-3999 Research reports,
2. **JAERI** 4001-5999 Survey reports and reviews,
3. **JAERI** 6001-6999 Information and Guiding Booklets.

Any inquiries concerning distribution copyright and reprint of the above reports should be derected to the Division of Technical Information, Japan Atomic Energy Research Institute, Tokai-mura, Naka-gun, Ibaraki-ken, Japan

編集兼発行　日本原子力研究所
印　　刷　科学図書印刷株式会社

# Oxidation Kinetics and Oxide Film Break-away of Zirconium and Its Alloys at High Temperatures


## Summary

The oxidation of Zr, Zircaloy-2, Zr binary alloys with Cu, Ni, Sn and Nb was studied with a particular emphasis on the mechanism of the rate transition in 600 to 850°C dry oxygen.

The results obtained from the continuous gravimetric measurements were compared with the oxide morphology involving hot-stage microscopy, X-ray and electron diffraction data, and electron beam micro probe analysis of the oxide-metal interfaces. No close relationship was found between the rate transition and either cracking or transformation of the oxide. A mechanism involving the recrystallization of the oxide is discussed based on a consistent relationship between the kinetic behavior and the behavior of the alloying elements during the oxidation. Stability of anion vacancies in $ZrO_2$ was pointed out as an important factor determining the rate transition.


March 1968


SUEO NOMURA and CHO AKUTSU
Division of JMTR,
Oarai Research Establishment,
Japan Atomic Energy Research Institute,


# 高温におけるZrとその合金の酸化動力学と酸化膜のbreakaway*


## 要　旨

純 Zr, Zircaloy-2 と Zr-Cu, Ni, Sn, Nb などの二元合金の 600～850°C の空気または純酸素中における酸化を，とくに反応速度の transition（遷移）を重点に研究した．

実験は連続記録式の熱天秤によっておこない，各時間における酸化膜の構造を X 線，電子廻折などによって解析すると共に酸化膜中の合金元素の分布を電子線マイクロアナライザーによって調べた．他方，酸化膜表面の割れの発生と成長を高温顕微鏡によって追跡した．

結果は酸化速度の transition をおこしにくいものとおこし易いものの二つの group に分れ，前者には純 Zr, Zr-Cu, Ni 合金，後者には Zircaloy-2, Zr-Nb, Zr-Sn 合金などが含まれる．前者の合金では metal-oxide の境界層に合金元素の濃縮化（選択酸化）がみられ，これに反して後者の合金では選択酸化はみられない．酸化速度の遷移の原因として今まで4つの説が提出されてきたが酸化物の再結晶説が最も各種の実験結果と一致することを示し，遷移は酸化膜中の anion vacancy が安定な時におこりにくいことを立証した．そして合金元素のイオン半径，酸化物半導体の型，原子価などとの関連を見出した．


1968年3月


日本原子力研究所　大洗研究所
材料試験炉部
野　村　末　雄
坏　　長


---

* この論文は1965年の電気化学会（アメリカ）主催のジルコニウムシンポジウムで発表され，*Electrochem. Tech.* **4** 93 (1966) に掲載された論文のうち紙数の関係で掲載できなかったものも含めた詳細全文である．

## Contents



## 目　　次

## 1. Introduction

Numbers of works[1~6] on high temperature oxidation of Zr and its binary alloys have been published. The oxidation kinetics, however, are not perfectly understood yet. In particular, the mechanism of the so-called break-away phenomenon——generally referred to as oxidation ratetransition has not been established yet, although several theories have been proposed.

Extending the early work by PORTE *et al.*[1], MISCH and DRUNEN[2] have classified pure Zr and 21 Zr binary alloys into 3 groups based on their kinetic behavior in high temperature oxidation. BAQUE *et al.*[3] tested various kinds of Zr and its binary and ternary alloys in high temperature $CO_2$. In reviewing the results reported by those 3 groups the following facts may be extracted.

i) Addition of a certain percent Cu to Zr gave the best oxidation resistance.

ii) Addition of Ni and Fe gave oxidation resistance equivalent to or better than that of pure Zr.

iii) Zr–certain % Cu and Zr–4% Ni alloys did not show the oxidation rate transition during 300, 000 minute tests in 700°C oxygen[2].

iv) Zr–Al, Zi–Sn and Zr–Nb alloys tended to have the rate transitions at comparatively early stages of oxidation and their oxidation resistance was much lower than that of pure Zr[1, 2, 3, 7].

The present authors have studied primarily on the mechanism of the oxidation rate transition using techniques of continuous weight gain measurements, hot stage microsopy, and X-ray and electron diffraction.

## 2. Expreimental methods

### 2. 1 Materials

**Unalloyed Zr.** Three kinds of unalloyed Zr were prepared; namely, arc-melt (reactor grade), electron-beam-melt (reactor grade), and arc-melt (commercial grade) Zr. The Zr specimens were furnished in the form of rolled sheet with the thickness of 1 mm. The specimens were chemically polished in a solution containing nitric acid and hydrofluoric acid after annealing at 750°C for 1. 5 hrs. and subsequent abrading with 800 grid emery paper.

All other alloy specimens described below received the same surface treatment.

**Zr–Cu alloys.** After being prepared through electron-beam melting, the specimens were shaped in the form of 1 mm thick sheets by cold rolling. In order to remove the segregation of Cu-rich phases, water quenching was applied after $\beta$–annealing for 15 hrs.

**Zr–2 wt. % Ni alloy.** An ingot was made by consumable electrode arc melting. The specimens were hot and cold rolled to 1 mm thick sheets and $\alpha$–annealed at 700°C for 1. 5 hr.

**Zr–Sn alloys and Zircaloy–2.** Zr–Sn alloy ingots were prepared through eletron-beam melting. 1 mm thick sheets, being formed by hot and cold rolling, were $\alpha$–annealed at

750°C for 1.5 hr. Zircaloy-2 was obtained from the market. They were arc-melted and rolled to 1 mm thick sheets. The subsequent treatments were the same as those for Zr-Sn alloys.

**Zr-2.5 wt. % Nb alloy.** An ingot was prepared by a double-melting method with consumable electrodes. The material was shaped in the form of a bar with 10 mm dia. by forging and the subsequent hot extrusion, and sliced to 1.5 mm thick disc. These specimens were annealed at 500°C for 1.5 hr. TABLE 1 summarizes the chemical compositions of the specimens used in the present study.

TABLE 1. Chemical composition of zirconium and its alloys (ppm)

| | Fe | Cr | Ni | Al | C | Si | Hf | N | O | H | Cu | Sn | Nb |
|---|---|---|---|---|---|---|---|---|---|---|---|---|---|
| Unalloyed Zr No. 1+ | 2,710 | 52 | 30 | 140 | – | 50 | 90 | 18 | 810 | 42 | – | – | – |
| 〃 No. 2++ | 1,720 | 77 | 30 | 50 | 40 | 35 | 82 | 31 | 630 | – | 40 | – | – |
| 〃 No. 3+++ | 1,050 | – | – | 490 | 55 | 15 | 2.50* | 50 | 2,030 | 57 | – | – | – |
| Sponge Zr | 517 | 99 | 30 | 44 | – | 30 | 81 | 15 | 932 | – | – | – | – |
| Zr-1% Cu | 320 | – | – | – | 40 | – | 79 | 12 | 560 | – | 0.66* | – | – |
| Zr-2% Cu | 280 | – | – | – | 20 | – | 70 | 10 | 710 | – | 1.56* | – | – |
| Zr-4% Cu | 340 | – | – | – | 30 | – | 77 | 18 | 770 | – | 3.30* | – | – |
| Zr-2% Ni | – | – | 1.95* | – | – | – | – | – | – | – | – | – | – |
| Zr-0.3% Sn | 900 | 32 | 30 | 65 | 30 | 64 | 98 | 34 | 750 | – | 40 | 0.25* | – |
| Zr-0.5% Sn | 430 | 30 | 30 | 55 | 40 | 24 | 95 | 26 | 860 | – | 40 | 0.37* | – |
| Zr-1% Sn | 500 | 18 | 30 | 40 | 30 | 34 | 96 | 24 | 410 | – | 40 | 0.81* | – |
| Zr-2.5% Nb | – | – | – | – | – | – | – | – | – | – | – | – | 2.47* |
| Zircaloy-2 | 1,700 | 60 | 60 | 56 | 40 | 60 | 70 | 28 | 770 | 21 | – | 1.39* | – |
| | Fe | Co | Ni | Al | C | Si | Ti | N | S | Tl | Cu | | Nb |
| (Ni) | 70 | 3,300 | Bal. | 100 | 40 | 100 | 100 | – | 700 | – | 10 | – | – |
| (Nb) | 100 –500 | – | – | – | 100 | 100** | 300 | 500 | – | 0.3* –1.5 | – | | Bal. |

Key ; * weight percent (%) ; ** $SiO_2$ ; + arc-melted reactor grade Zr ; ++ electron-beam melted reactor grade Zr ; +++ arc-melted commercial grade Zr ; Zr-2% Ni and Zr-2.5% Nb were prepared from sponge Zr.

## 2.2 Experimental Procedure

**Kinetic measurements.** An ORK autorecording thermo-balance (Oyo Rika Co.) was used for the continuous gravimetric measurements on 15×30×1 mm specimens.

Commercially pure oxygen was used as the oxidation environment being supplied from a tank via a $P_2O_5$ desicator train. Air was used in a limited number of runs. The system was maintained at atmospheric pressure throughout the tests.

**Microscopic observation.** The surfaces and cross sections of oxidized specimens were examined with an optical microscope at various stages of oxidation. A hot-stage microscope (HUM Union Optics Co.) was used in observing dynamically the oxide growth and the formation and propagation of cracks.

Oxygen was continuously replenished through the hot stage at 700°C.

The surfaces of specimens were examined at various stages with an electron microscope for which the standard plastic-replica technique was used.

**Electron and X-ray diffraction analysis** Surface oxide films were removed by dissolving the underlying metal according to EVAN's method[8]. Both sides of the isolated oxide film were examined by surface electron diffraction. The same oxide specimens were examined by X-ray

diffraction to obtain their bulk crystal structures.

**Electron beam micro probe analysis.** The surfaces and cross sections of the specimens were analyzed before and after oxidation tests by means of an XMA (X-ray Micro Analyzer, NDK Co.). Line scanning and characteristic X-ray images were obtained for those elements which were alloyed with Zr.

## 3. Results

### 3. 1 Kinetic Measurements

Two measurements were made for each type of specimen in the temperature range 600 to 850°C. **Fig. 1** (a)～(h) shows some of the typical measurements. **TABLE 2** is a summary of

**TABLE 2** Kinetic constants of Zr and its alloys during oxidation

| Materials | Atmosphere | $1/n$ at pre-transition | | | | Time to rate transition | | | | Weight gain at transition | | | |
|---|---|---|---|---|---|---|---|---|---|---|---|---|---|
| | | 850°C | 800°C | 700°C | 600°C | 850°C | 800°C | 700°C | 600°C | 850°C | 800°C | 700°C | 600°C |
| Unalloyed Zr No. 1 | $O_2$ | 0.41 | 0.40 | 0.37 | 0.36 | 450 | 550 | * | * | 420 | 350 | * | * |
| | Air | – | – | 0.40 | – | – | – | – | – | – | – | – | – |
| Zr No. 2 | $O_2$ | 0.38 | 0.40 | 0.35 | 0.38 | * | * | * | * | * | * | * | * |
| Zr No. 3 | $O_2$ | – | 0.46 | 0.45 | 0.44 | – | 570 | 820 | 910 | – | 1020 | 1000 | 800 |
| Zr–1% Cu | $O_2$ | – | 0.46 | 0.39 | 0.36 | – | * | * | * | – | * | * | * |
| Zr–2% Cu | $O_2$ | 0.49 | 0.49 | 0.40 | 0.36 | * | * | * | * | * | * | * | * |
| Zr–4% Cu | $O_2$ | – | 0.50 | 0.45 | 0.39 | – | * | * | * | * | * | * | * |
| Zr–2% Ni | $O_2$ | – | 0.41 | 0.32 | 0.34 | – | * | * | * | – | * | * | * |
| Zr–2.5% Sn | $O_2$ | – | 0.53 | 0.44 | 0.44 | – | 150 | 520 | 1300 | – | 920 | 780 | 410 |
| Zr–0.5% Sn | $O_2$ | – | 0.41 | 0.41 | 0.42 | – | 600 | 450 | 1050 | – | 400 | 190 | 132 |
| | Air | – | 0.42 | 0.46 | 0.45 | – | 430 | 660 | 1230 | – | 385 | 245 | 105 |
| Zr–1% Sn | $O_2$ | – | 0.46 | 0.43 | 0.50 | – | 330 | 490 | 710 | – | 400 | 240 | 90 |
| | Air | – | 0.45 | 0.43 | 0.49 | – | 375 | 540 | 610 | – | 350 | 250 | 94 |
| Zircaloy–2 | $O_2$ | 0.38 | 0.51 | 0.41 | 0.33 | 140 | 147 | 110 | 690 | 430 | 265 | 85 | 90 |
| | Air | – | 0.50 | 0.34 | 0.33 | – | 180 | 120 | 590 | – | 240 | 107 | 85 |

Key ; * transition did not occur, – : not measured ; time to transition (min.) ; weight gain ($mg/dm^2$)

the obtained kinetic data involving the weight gains, the times to transition and the values of "$n$" assuming that the weight gain ($W$, $mg/dm^2$) is expressed as a function of time, namely $W=kt^n$, where $k$ and $n$ are the rate constant and the exponent index respectively.

### 3. 2 Correlation between the Kinetic Behavior and the Oxide Morphology

**Fig. 2** shows the kinetic behavior of pure Zr (No. 1) and zircaloy–2 and their corresponding surface appearance.

Optical micrographs of the cross sections of these specimens taken under polarized illumination are shown in **Fig. 3.** It is seen in these figures that the pure Zr specimen does not suffer a rate transition and its protective black oxide grows steadily ; while in the zircaloy–2 specimen, the black oxide turns white abruptly at the rate transition point, leaving a thin layer of the

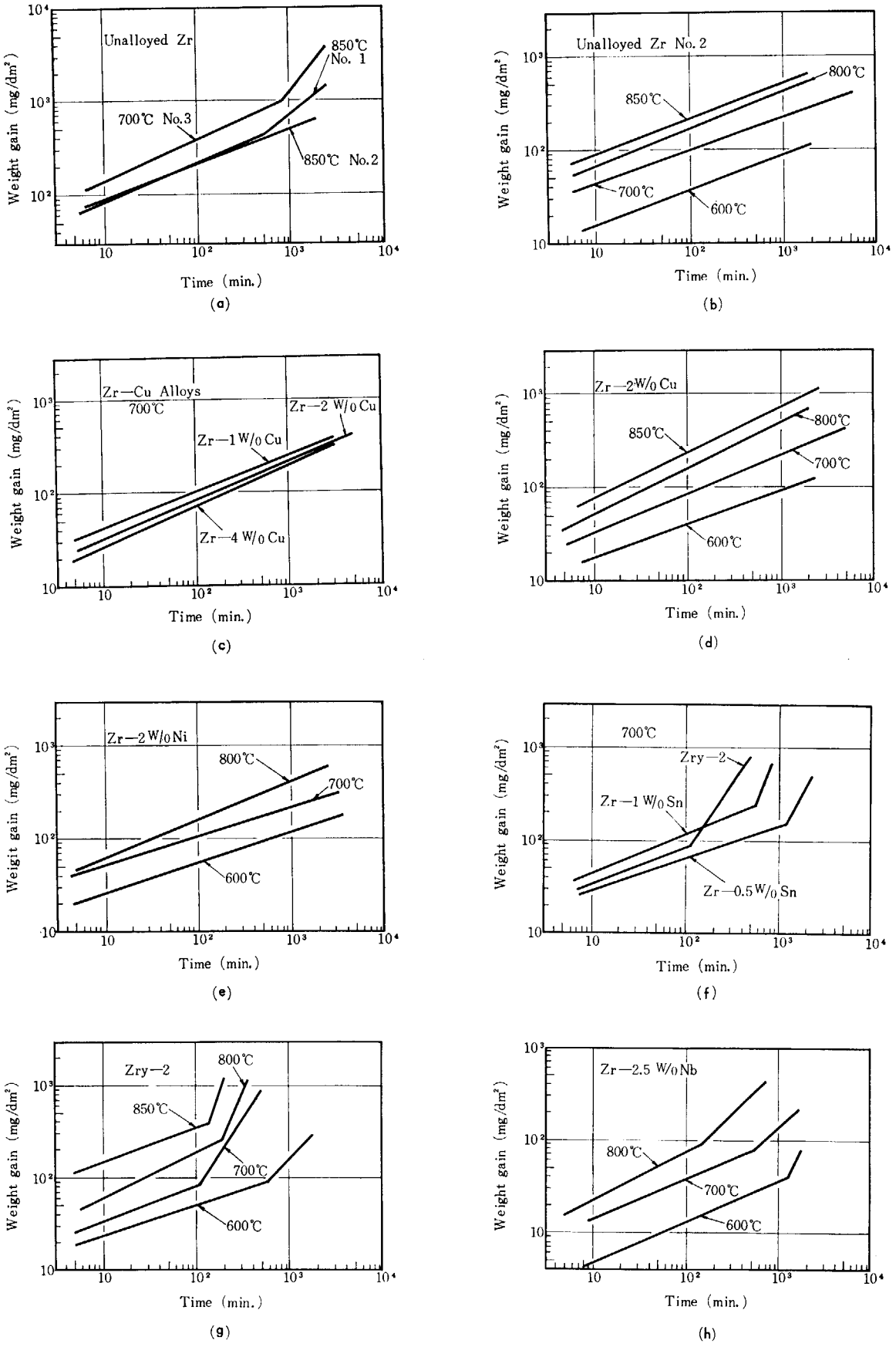


**Fig. 1** Oxidation of zirconium and zirconium alloys in oxygen.

black oxide at the oxide-metal interface. This thin black layer stays at an almost constant thickness during the subsequent period of oxidation.

Assuming that the oxidation process is controlled by the inward diffusion of $O^{-2}$ through this black layer, the observed transition may be interpreted in terms of the change of the value $n$ from $n=1/2$ to $n=1$. The behavior of Zr-Cu and Zr-Ni alloys were basically similar to that of the pure Zr specimen while Zr-Sn and Zr-Nb alloys behaved similarly to the zircaloy-2 specimen.

### 3. 3 Hot Stage Microscopy of Oxidizing Surfaces

Fig. 4 shows micrographs of the surfaces of Zr-2 wt% Cu, pure Zr (No. 1), zircaloy-2, and Zr-2.5 wt% Nb specimens taken during the high temperature oxidation process. In these pictures, the progression and propagation of oxide cracks are readily visible.

Electron microscopic observation revealed a number of micro fissures along the grain boundaries of all the specimens tested even at very early stages of oxidation. These fissures are not detected with optical microscopes. A similar observation has been reported by Cox[9]. These micro fissures do not grow appreciably in Zr-Cu alloys in the subsequent oxidation. On the other hand the fissures grow substantially in the pure Zr specimen to form a network of cracks extended over the entire surface of the oxide after 2000 min., and the oxide tended to spall at a later stage. The micro fissures in the zircaloy-2 specimens did not show any substantial growth in the stages before and after the rate transition point, but they extended abruptly to form crack-networks well after the transition point (1000 min.).

In Zr-2.5 wt% Nb alloy specimens, the growth of cracks became pronounced (200 min.) before the rate transition. Crack-networks were subsequently formed.

No consistent correlation between the rate transition and the oxide film cracking was observed in the hot-stage microscopic study. Therefore it would not be proper to attribute these two phenomena to the same cause.

### 3. 4 Structural Study of the Oxide Film

Oxide films were isolated in their descrete form by dissolving the underlying metal. Both sides of these films were then examined by surface electron diffraction. TABLE 3 summarizes the surface diffraction data and the bulk X-ray diffraction data.

No strict correlation between the oxide structure and the rate transition could be detected in these data. Consequently, the mechanism[10] which attributes the rate transition to the cubic-

TABLE 3 Crystal structures of oxides formed on zirconium and its alloys

| | | Unalloyed Zr | Zr-2% Cu | Zr-2% Ni | Zircaloy-2 | | Zr-2.5% Nb | |
|---|---|---|---|---|---|---|---|---|
| | | | | | Pre-trans. | Post-trans. | Pre-trans. | Post-trans. |
| X-ray diffraction | | M | M | M | M | M | M | M |
| Surface electron diffraction | (I) | C | C | C | C | C | C | C |
| | (II) | C | C | C | M | M | C | C?(Halo) |

Key; M: Monoclinic structure; C: Cubic or tetragonal structure.
(I): Inner surface of oxide (metal-oxide interface).
(II): Outer surface of oxide (oxide-gas interface).

monoclinic transformation of $ZrO_2$ would not be strictly realistic.

### 3. 5 Electron Beam Micro Probe Analysis

The results of line scanning and characteristic X-ray images ($K_\alpha$ or $L_\alpha$) of the cross sections of oxidized specimens are summarized in **Fig. 5.** Two features are distinguished in Zr -Cu and Zr-Ni alloys, (1) neither Cu nor Ni dissolves appreciably in the oxide, and accordingly (2) a Cu- or Ni-rich layer is formed at the metal side of the oxide-metal interface. On the other hand, Sn and Nb, in zircaloy-2 and Zr-2. 5 wt. % Nb alloy, respectively, occurred in the $ZrO_2$ phase in the same concentrations equivalent as those present in the unoxidized materials. The same was true for Zr-Sn and Zr-Al alloys.

A couple of micro hardness indentations (Vickers) served as markers on the specimen surfaces to locate the positions of line scannings before and after the oxidation. The positions were approximately the same. Typical results are illustrated in **Fig. 6.**

**Fig. 6** indicates that the oxide film on Zr-2 wt.% Cu alloy contains Cu-rich regions locally,

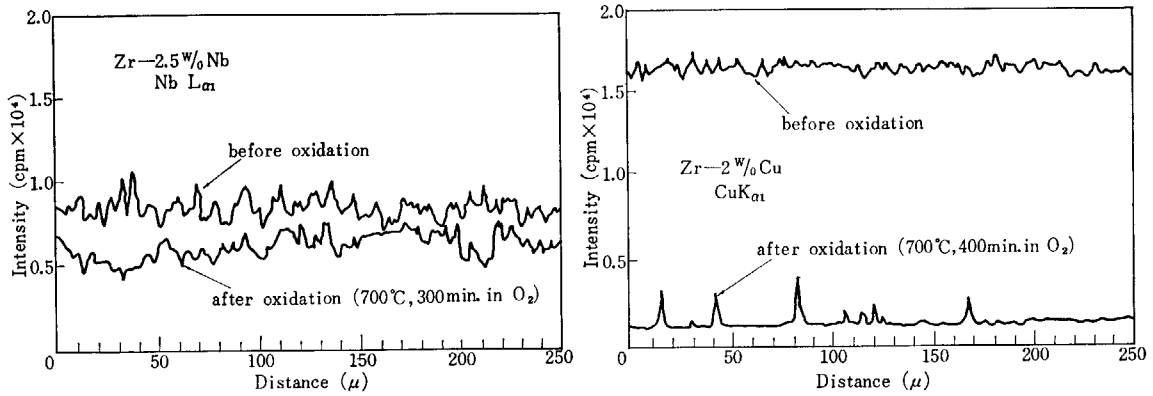


**Fig. 6** Characteristic X-ray line scanning of alloy surface.

even though the bulk oxide does not dissolve Cu appreciably. In contrast, Nb is uniformly dissolved in the oxide film on Zr-2. 5 wt.% Nb alloy.

Within the ranges of compositions used in the present study the Zr-Ni alloy behaved similarly to the Zr-Cu alloys while Zr-Sn alloys and zircaloy-2 closely resembled to the Zr-Nb alloy. These two typical tendencies are substantially consistent with the two categories of classification for the kinetic behavior of these alloys. It is therefore suggested that in the range of the present study those elements that fail to dissolve in the $ZrO_2$ film and thus tend to accumulate at the oxide-metal interfaces delay the oxidation rate transition of Zr in dry oxygen, while those with higher solubilities in the oxide tend instead to induce the transition.

## 4. Discussion

**Fig. 1** (a) indicates that the oxidation resistance of unalloyed Zr is enhanced by increased purity. Below 850° C the two reactor-grade pure Zr specimens did not differ appreciably in oxidation resistance. The difference became appreciable when the test temperature was shifted to 850° C. Although the difference in oxidation resistance may be attributed partly to the purity

of the metal, the second phase distribution, as seen in **Fig. 7**, is more likely to play a principal role. It has been found by COX[9] and the authors[11] that a fine distribution of the second phase gives an improved oxidation resistance and retards oxide film break-away on zircaloy. A similar effect has been recognized by BOYD[12] on unalloyed Zr.

The three currently proposed mechanisms of the oxidation rate transition (generally referred to as the oxide film break-away) have been classified by COX[9] as follows:

1) The first group proposes that the transition of the nonstoichiometric black oxide into the stoichiometric white oxide is not a result but the cause of the oxide fracturing. The change of stoichiometry is explained in terms of the saturation of the oxide film[13, 14] or of the underlying metal phase[15] with oxygen. Embrittlement of the underlying metal phase[4, 16] is also pointed out.

This group considers oxygen diffusion through the oxide layer and/or the underlying metal; accordingly the time to rate transition (will call *tr* hereafter) would be determined only by oxygen diffusion. There would be expected to be longer *tr* as the thickness of the specimen sheet is increased. However, the authors' results[17] showed that the 0.4 mm thick specimens always had a longer *tr* than the 0.1, 0.2, 0.8, and 1.5 mm thick specimens in 600, 700 and 800°C oxygen. TAKAMURA[18] reported similar results.

The authors have measured the hardnesses of the cross sections of various types of specimens to justify their concept that the rate transition is induced when the underlying metal phase in the immediate vicinity of the oxide-metal interface reaches a critical stage where the embrittlement of the metal causes cracking. Those specimens which had already experienced break-away showed somewhat lower hardnesses near the oxide-metal interface than those alloy or pure metal specimens in the state without break-away. This seems to suggest that attention should be focused on a change of the oxide film itself.

That the oxide visibly turns white during the rate transition provides experimental evidence that the nonstoichiometric black oxide turns abruptly into the stoichiometric white oxide. Therefore an explanation of the rate transition only in terms of oxygen diffusion may not be adequate.

2) The second group attributes the transition to a crystallographic change in the oxide, namely the transformation of cubic or tetragonal $ZrO_2$ into the more stable monoclinic form. The results shown in **TABLE 3** do not support this idea. COX[9] also disagrees.

3) The third group considers the rate transition in terms either of (a) a mechanical fracturing of the oxide film or (b) a change of the properties of the oxide due to recrystallization. The former, (a), is not substantiated, since the result in **Fig. 4** indicates no correlation between the cracking of the oxide film and the commencement of the rate transition.

WALLWORK *et al.*[19], studying Zr oxidation at 850°C and 950°C, observed a correlation between the rate transition and the formation of cracks due to stresses around the interface between the two phases, namely, oxide and metal-oxygen solid solution. They also observed the formation of voids at the oxide-metal interface and the recrystallization of the metal in the immediate vicinity of the interface.

It might be expected that the stress raised at the oxide-metal interface would play an important role in the rate transition; however, neither voids formation nor recrystallization of underlying metal was observed in any of the specimens at the temperatures used in the present study.

BIBB and FASCIA[20] and HAYCOCK[21] report changes in the properties of the oxide due to

its recrystallization. The former proposed a mechanism of the rate transition on the basis of their results of aquaous corrosion tests on Zr single crystals at 360° C. They think that a strain induced recrystallization or fragmentation of oxide accompanies the change from a protective black oxide to a nonprotective white oxide. HAYCOCK[21] also stresses the relationship between the recrystallization of the oxide and a change in the kinetics. The present authors also consider that oxide recrystallization is the most likely cause of the rate transition.

The mode of occurrence resembles that of recrystallization in such a way that the abrupt change commences after a pre-transition (incubation) period, and this period becomes shorter as the temperature is increased, although the nature of recrystallization in ceramic materials such as oxide is not well defined[22]. Nevertheless no known phenomenon is inconsistent with the oxide recrystallization mechanism.

Assuming that recrystallization of oxide is a major cause of the rate transition and that temperature, strain and impurity content are the principal factors affecting the recrystallization, as is the case for most metals, the following argument is proposed.

Consider the interfacial stress as one of the principal factors. A compressive stress is raised in $ZrO_2$ since it has a larger specific volume than Zr. Since the growth of Zr-oxide film is known as a oxygen inner-diffusion mechanism in this system, the compressive stress will be greatest at the place closest to the oxide-metal interface. If a number of stable vacancies exist in the oxide, particularly in the vincinity of the oxide-metal interface, these vacancies may act as stress relievers which retard the rate transition. On the other hand, these vacancies will be favorable to the stability of the black nonstoichiometric oxide. As long as the black nonstoichiometric oxide remains stable, the rate transition does not take place. In other words the stability of the black oxide is favored by large number of stable oxygen anion vacancies in the oxide, and the resultant stress relief, then, tends to retard the rate transition.

O' DRISCOLL *et al.*[4] found that nitrogen-rich Zr has a retarded rate transition.

The fact that pure Zr has a comparatively good resistance to the rate transition despite its high oxidation rate at higher temperatures may be explained reasonably in terms of its tendency to form more anion vacancies.

According to C. WAGNER's THEORY[23], alloying elements that have lower valences than $Zr^{+4}$ would favor the formation of anion vacancies, since $ZrO_2$ is an anion deficient n-type semiconductor. By this theory the retardation of the rate transition may be expected in $Cu^{+2\,or\,+1}$ and $Ni^{+2\,or\,+3}$ alloys, while $Al^{+3}$ and $Sn^{+3}$ alloys contradict it. The contradiction seen in the latter case suggests that not only the number of anion vacancies but also their stability, ionic radii and solubilities in the $ZrO_2$ matrix must be taken into account if the interfacial stress is a major factor.

PORTE *et al.*[1] pointed out that the difference in the ionic radii between an alloying element and Zr plays a major role in determing the length of *tr.* The above statement, indeed, agrees with the fact that Sn, Nb and Al differ from Zr more in ionic radii than Ni and Cu. Furthermore, the elements in the former group have high solubilities (**Fig. 5**) in $ZrO_2$.* Hence, a larger stress can be raised in the former group alloys. This induces recrystallization, i.e., the rate transition.

PORTE used GOLDSCHMIDT'S ionic radii in his discussion. Using PAULING'S ionic radii, the radii of $Cu^{+}$ and $Zr^{+4}$ would differ more than $Sn^{+3}$ and $Zr^{+4}$. An additional difficulty arises when one considers why Zr-Cu alloys are superior to all others in spite of the fact that the ionic radius of $Ni^{+2}$ is closer to $Zr^{+4}$ than is that of $Cu^{+}$. The preceding indicates that ionic

* Recent work has found a large amount of Al dissolved in the oxide film.

radius may not be so important as Porte stresses.

**Fig. 5, 6** indicate that Cu (and Ni) do not dissolve much in the oxide, and that their distribution is not uniform. Some regions are extremely concentrated with these elements (perhaps as $Zr_2Cu$ or ZrCu). A Ni- or Cu-rich layer is formed at the metal side of the oxide-metal interface, where the stress is greatest.

Although the argument is still speculative, the combination of $ZrO_2$ and $Cu_2O$ (or NiO) such as that in **Fig. 8 (B)** is considered more likely than that in **Fig. 8 (A)**.* Since $Cu_2O$ and NiO are metal deficient p-type semiconductors, they will form more stable Shottky type defects when combined with n-type anion deficiet $ZrO_2$. Another type of stable vacancies, such as in **Fig. 8 (c)**, is also conceivable if there is electron exchange between $ZrO_2$ and $Cu_2O$. In such a case, $Zr^{+3}-e\rightarrow Zr^{+4}-9.8\,eV$, $Cu^{+2}+e\rightarrow Cu^{+}+12.6\,eV$ and $Ni^{+2}+e\rightarrow Ni^{+}+10.6\,eV$. Thus, $Zr^{+3}+Cu^{+2}\rightarrow Zr^{+4}+Cu^{+}+2.8\,eV$ and $Zr^{+3}+Ni^{+2}\rightarrow Zr^{+4}+Ni^{+1}+0.8\,eV$ are obtained respectively. This means that this type of reaction is fairly probable.

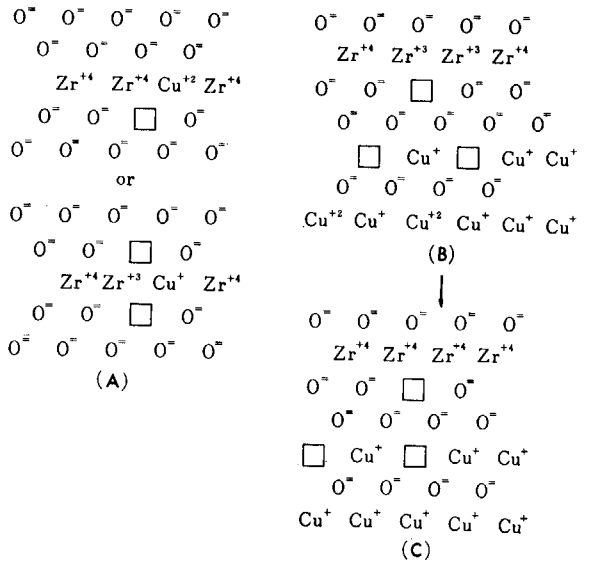


(A) Wagner type
(B) Combination of both oxides
(C) Modification of (B)

**Fig. 8** Schematic representation of vacancies in oxide of Zr–Cu alloy.

A suggested distribution of CuO or $Cu_2O$ in $ZrO_2$ film is shown in **Fig. 9.** A suitable distribution of strongly anchored vacancies in the Zr-Cu (or Zr-Ni) alloys may account for the fact that the black oxide does not easily turn white, and stable vacancies are formed particularly at the Cu rich metal-oxide interface through the stress relaxation mechanism described above.

The fact that the oxide-metal volume ratios for Cu and Ni ($Cu_2O/Cu=1.64$, $NiO/Ni=1.65$) are close to that for Zr ($ZrO_2/Zr=1.56$) may also contribute to the retardation of the rate transition, because stress concentration will be not much at the boundary between $ZrO_2$ and

* If the model in **Fig. 8 (A)** were more likely, Cu would dissolve in the oxide more uniformly and would show the characteristic X-ray image as Sn and Nb do. Hence we would expect a much reduced difference in the oxidation resistance between Zr-Cu and Zr-Sn alloys.

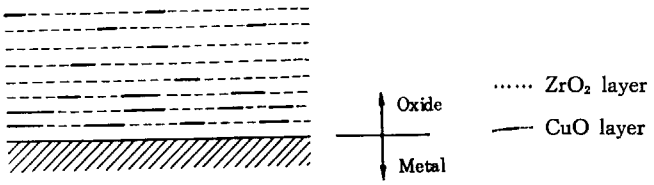


**Fig. 9** Suggested distribution of Cu oxide layer in Zr oxide film.

$Cu_2O$ (orNiO) layers.

In view of the above discussion those alloying elements which may contribute to the retardation of the rate transition of Zr must satisfy the following conditions:

(1) They should have a lower valency than $Zr^{+4}$

(2) They should have ionic radii close to that of Zr

(3) They should be less soluble in $ZrO_2$

(4) They should form metal deficient semiconductors

**TABLE 4.** Comparison of properties of alloying elements with those of Zr

| | Valency | Ionic radii[1] | $\alpha$-solubility in Zr metal[2] | Type of oxide semiconductor[3,4] | Metal/oxide sp. volume ratio[3] |
|---|---|---|---|---|---|
| $Cu^{+}$ | A | B | A | A | A |
| $Cu^{+2}$ | A | A | A | B | A |
| $Ni^{+2}$ | A | A | A | A | A |
| $Co^{+}$ | A | A | A | A | B |
| $Cr^{+3}$ | A | B | A | A | C |
| $W^{+4}$ | B | A | A | A | C |
| $Hf^{+4}$ | B | A | * | C | A |
| $Fe^{+2}$ | A | A | A | A | C |
| $Fe^{+3}$ | A | B | A | C | C |
| $Be^{+2}$ | A | C | A | C | A |
| $U^{+4}$ | B | B | A | B | C |
| $Mo^{+4}$ | B | A | A | A | C |
| $Ta^{+2}$ | C | A | ? | C | C |
| $V^{+4}$ | B | B | A | C | C |
| $Ti^{+4}$ | B | A | * | C | B |
| $Nb^{+5}$ | C | A | C | C | C |
| $Sn^{+4}$ | B | A | C | C | B |
| $Pb^{+4}$ | B | A | C | C | B |
| $Al^{+3}$ | A | C | C | C | A |

1) by AHRENS (1952), 2) LUSTMAN & KERZE "Metallurgy of Zr,"
3) KUBASCHEWSKI & HOPKINS "Oxidation of Metals and Alloys,"
4) KAWAGUCHI "Chemistry of semi-conductor"

Foot Note:

| | A | B | C | |
|---|---|---|---|---|
| Valency | <4 | 4 | >4 | |
| Ionic radii | 0.68–0.92 Å (15%) | 0.63–0.67 Å<br>0.93–0.97 Å | <0.63 Å<br>>0.97 Å | |
| $\alpha$-Solubility+ | 0.5% | 0.5~3% | 3% | *Solid solution |
| Type of oxide semi-conductor | Metal-deficit | Amphoteric | Metal-excess | |
| Oxide/metal ratio | 1.40–1.72 (10%) | 1.25–1.39 (20%)<br>1.73–1.87 (20%) | <1.25<br>>1.87 | |

+ Solubility of an alloying element in Zr oxide can be generally dealt similarly to its $\alpha$-solubility in Zr metal.

(5) They should have oxide-metal volume ratios close to or less than 1.56

TABLE 4 compares various alloying elements with respect to the above five requirements. These elements are arranged in the order of the length of the pretransition period (*tr.*), based on the experimental results by MISCH[2] and PORTE[1]. For W, Mo, and Cr the resistance is largely dependent on the alloy concentration, and these elements are only effective at lower concentrations; therefore, the data were taken conveniently from alloys containing around 1% of these elements. From TABLE 4 it is clear that conditions (1) to (5), particularly (3) and (4), are better satisfied by the elements with longer time to the rate transition.

## 5. Conclusions

From the experimental results and the above discussions the following conclusions can be stated:

1. Those specimens of which nonstoichiometric black oxide is stable are resistant to the rate transition. The thickness of the black oxide determines the oxidation rate.
2. The oxide film cracking does not have a strict relation to the rate transition.
3. No correlation between the rate transition and the transformation of $ZrO_2$ was observed.
4. The materials tested in the present study can be classified in two groups with respect to their kinetic behavior and the distribution of alloying elements in the metal and oxide phases. Those elements which have low solubilities in $ZrO_2$ delay the rate transition and tend to accumulate in the metal side of the oxide metal interfaces.
5. A mechanism of the rate transition, which involves strain induced recrystallization of $ZrO_2$ and the resultant change in the oxide properties, is shown to be the most likely one.
6. The stability of the nonstoichiometric black oxide was interpreted in terms of the stability and distribution of anion vacancies in $ZrO_2$ phase. These defects are considered to act as the stress relievers of oxide-metal interface regions.
7. The effect of alloying elements were explained in terms not of the impurity effect in semiconductors but of stabilization of defects in $ZrO_2$.
8. The 5 factors affecting the effect of alloying elements on the oxidation rate transition of Zr are pointed out: they are valency, ionic radius, solubility in $ZrO_2$, types of their oxide-semiconductors and oxide-metal volume ratios for the elements to be added to Zr.

## Acknowledgements

The authors wish to express their appreciation to Messers N. ITO and T. KIMURA for helping the experiments; and to Dr. T. KONDO for the discussions and the English translation.

A special thanks are given to Messers K. IZUI and S. FURUNO for doing the electron beam micro probe analysis. The supply of the specimen materials by Hitachi Ltd. and Kobe Steel Work Co. is gratefully acknowledged.

## References

1) H.A. PORTE, J.G. SCHNIZLEIN, R.C. VOGEL and D.F. FISCHER; *J. Electrochem. Soc.*, **107**, 506 (1960)

2) R.D. MISCH and C. VAN DRUNEN : GEAP-4089, Vol. 2, No. 15 (1962)
3) P. BAQUE, R. DOMINGET et J. BOSSARD : Rapport C.E.A. n° 2393 (1963)
4) W.G. O' DRISCOLL, C. TYZACK and T. RAINE : Second U.N. Conference on the Peaceful Uses of Atomic Energy, Paper No. 15/1450 (1958)
5) B. LUSTMAN and F. KERZE Jr. : Metallurgy of Zirconium, McGraw-Hill Book Co., New York (1955), p. 598
6) T. MAEKAWA and S. ISHI : *Trans. Jap. Inst. Metal.*, **24**, 608 (1960)
7) M.W. MALLET and W.M. ALBRECHT : *J. Electrochem. Soc.* **102**, 407 (1955)
8) U.R. EVANS and R. TOMLINSON : *J. Appl. Chem.*, **2**, 105 (1952)
9) B. COX : Progress in Nuclear Energy, Series 4, Vol. 4, Technology, Engineering and Safety, Pergamon Press (1961), pp. 177–184
10) I.I. KOROBKOV, D.V. IGNATOV, A.I. YEVTYUKIN and V.S. Yemelyanov, Second U.N. Conference on the Peaceful Uses of Atomic Energy, Paper No. 14/2054 (1958)
11) S. NOMURA and N. ITO : JAERI 1116 (1966)
12) W.K. BOYD, D.J. MAYKUTH, R.S. PEOPLES and R.J. JAFFE, BMI-1056 (1955)
13) S.B. DALGAARD : Interem report of Atomic Energy of Canada Limited, Met I-27 (1959)
14) E.S. SARSIKOV, N.T. CHEBOTAREV, A.A. NEVZOROVA and A.I. ZVERKOV, *Atomnaya Energiya*, **5**, 550 (1958)
15) K. OSTHAGEN and P. KOFSTAD : *J. Electrochem. Soc.*, **109**, 204 (1962)
16) J.P. PEMSLER : *J. Electrochem. Soc.*, **105**, 315 (1958)
17) S. NOMURA and KEE WON CHUN : to be published soon in Japan Atomic Energy Research Institute Report (JAERI-Report)
18) J. TAKAMURA : private communication.
19) G.R. WALLWORK, C.J. ROSA and W.W. SMELTZER : *Corrosion Sci.*, **5**, 113 (1965)
20) A.E. BIBB and J.R. FASCIA : Trans. AIME, **230**, 415 (1964)
21) E.W. HAYCOCK : *J. Electrochem. Soc.*, **106**, 771 (1959)
22) W.K. KINGERY : Introduction to Ceramics, John Wiley & Sons, Inc. (1960), p. 354
23) C. WAGNER : *Z. Physik. Chem.*, **B. 21**, 25 and **B. 22**, 181 (1933)

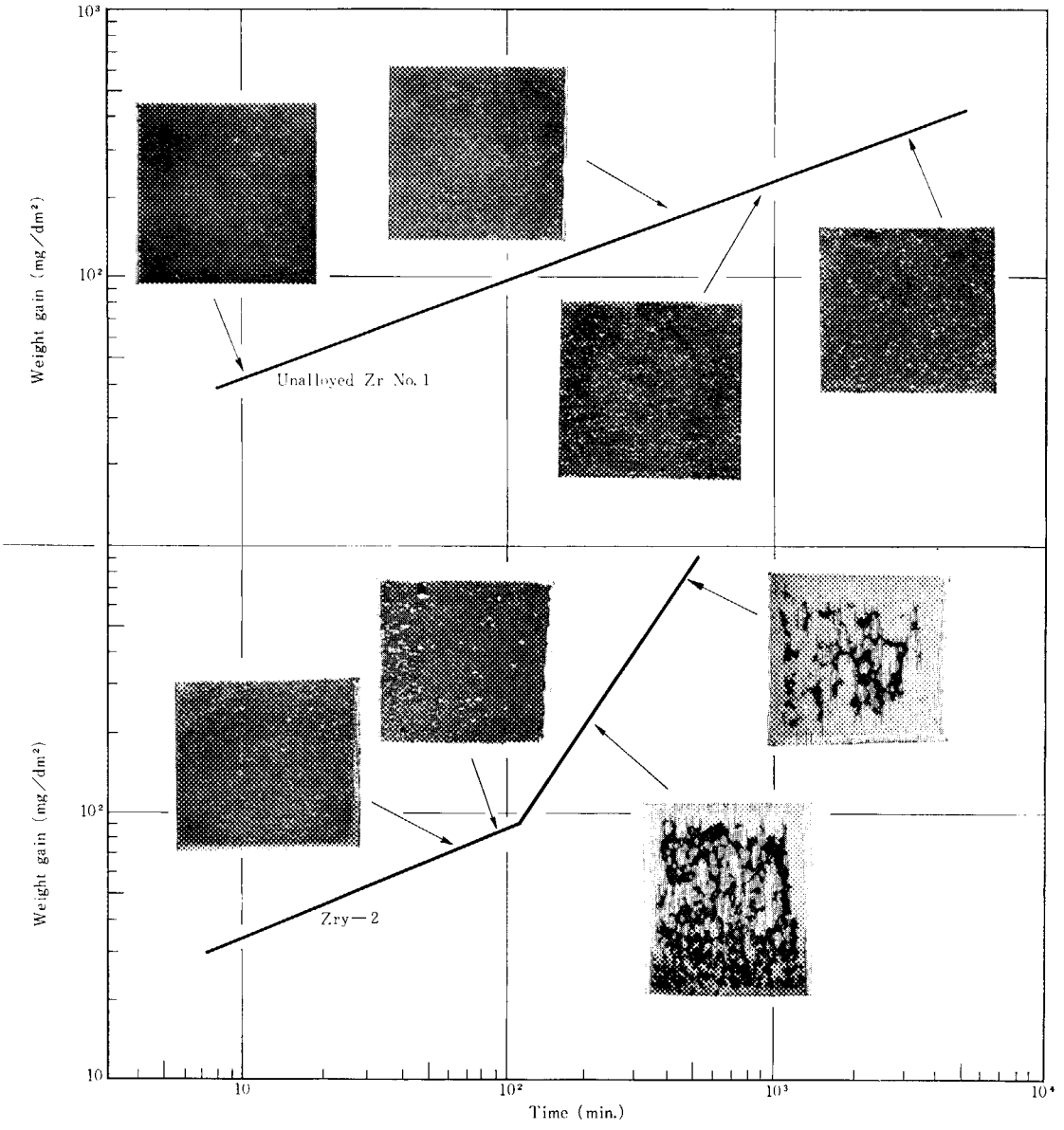


**Fig. 2** Macroscopic view of Zr and Zry-2 during oxidation in air at 700°C.

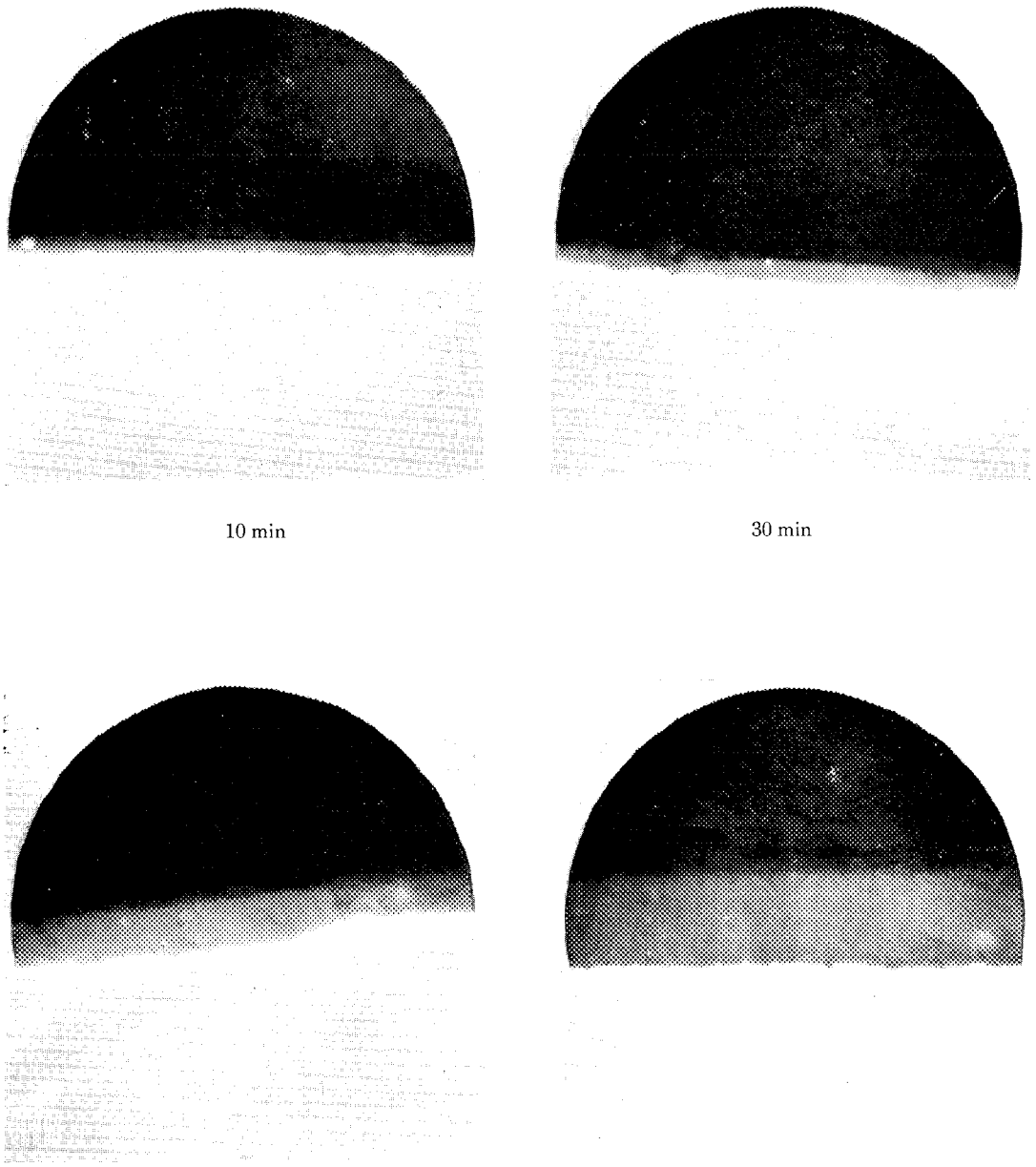


(a)

**Fig. 3** Cross section of oxide on unalloyed zirconium No 1 and zircaloy-2 (polarized light)

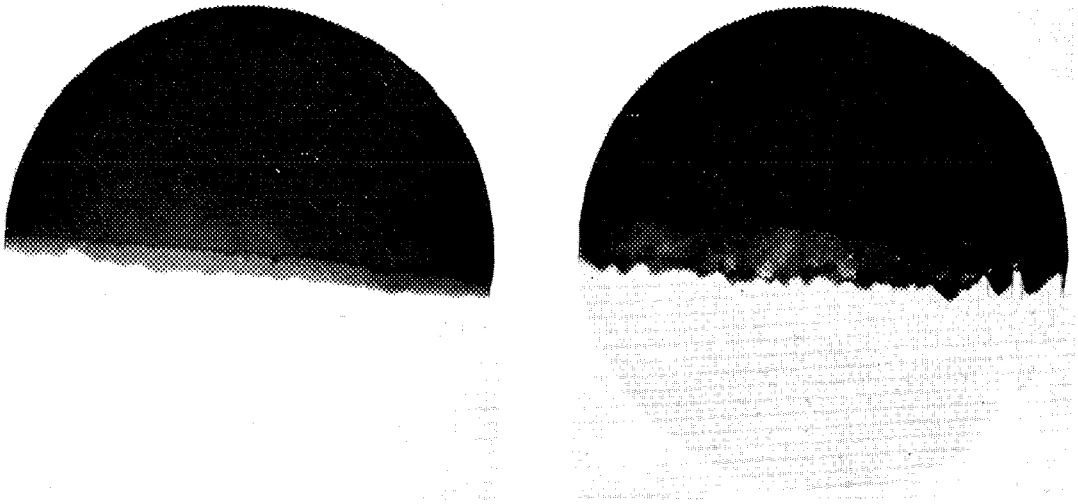

30 min 110 min

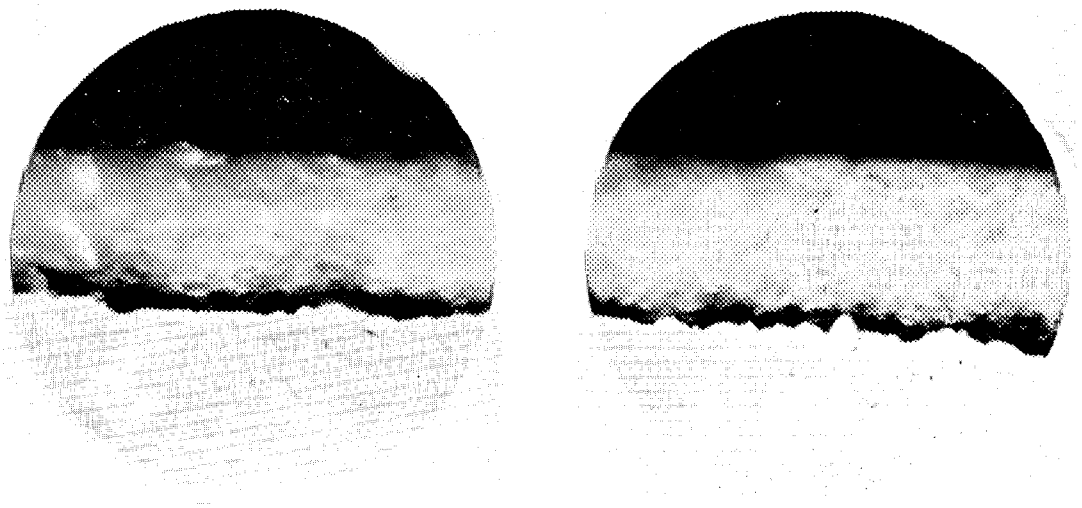

200 min 330 min ×840

( b )

( a ) Unalloyed zirconium No. 1 (700°C, in air)

( b ) Zircaloy-2 (700°C, in air)

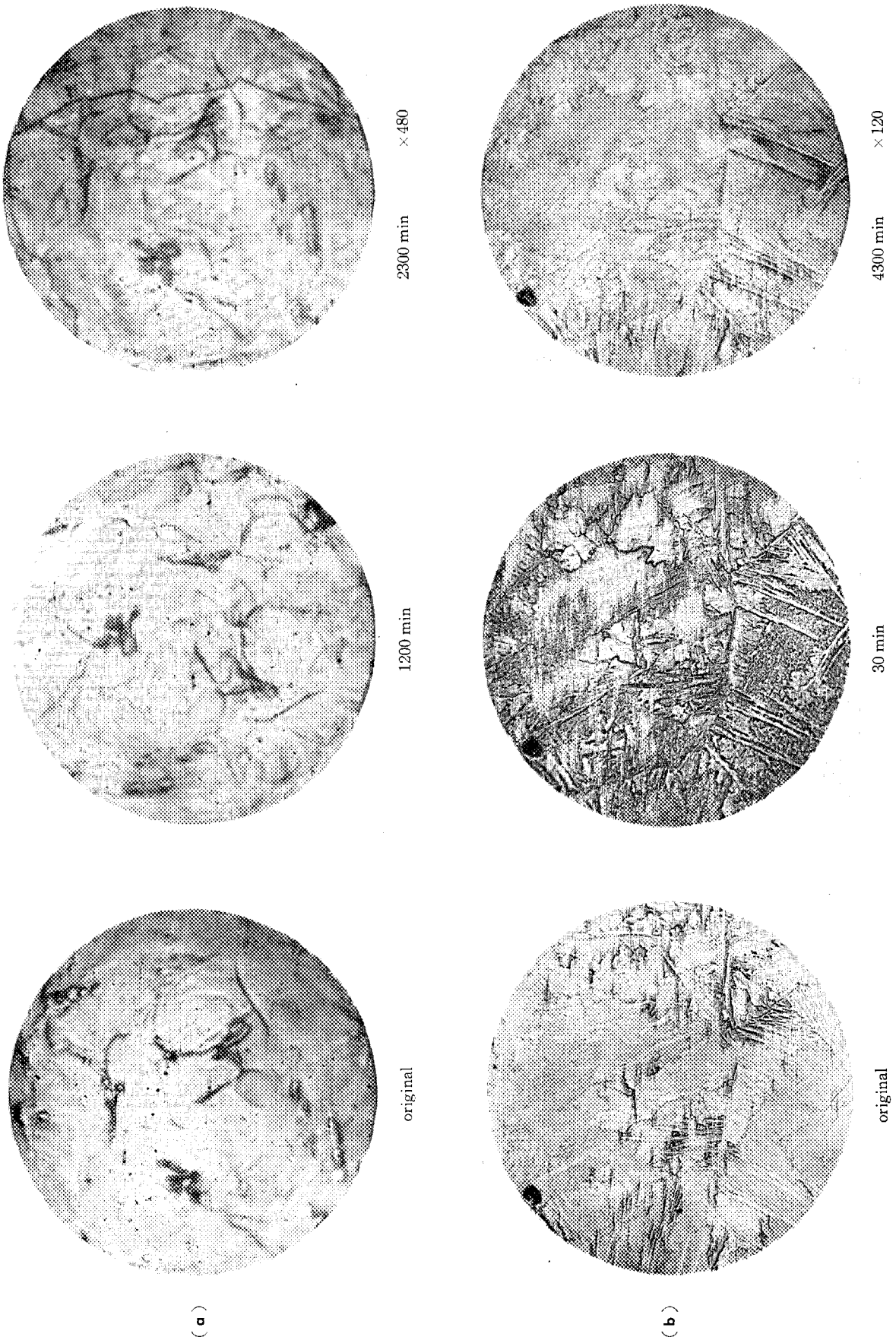
original
1200 min
2300 min
×480
(a)
original
30 min
4300 min
×120
(b)

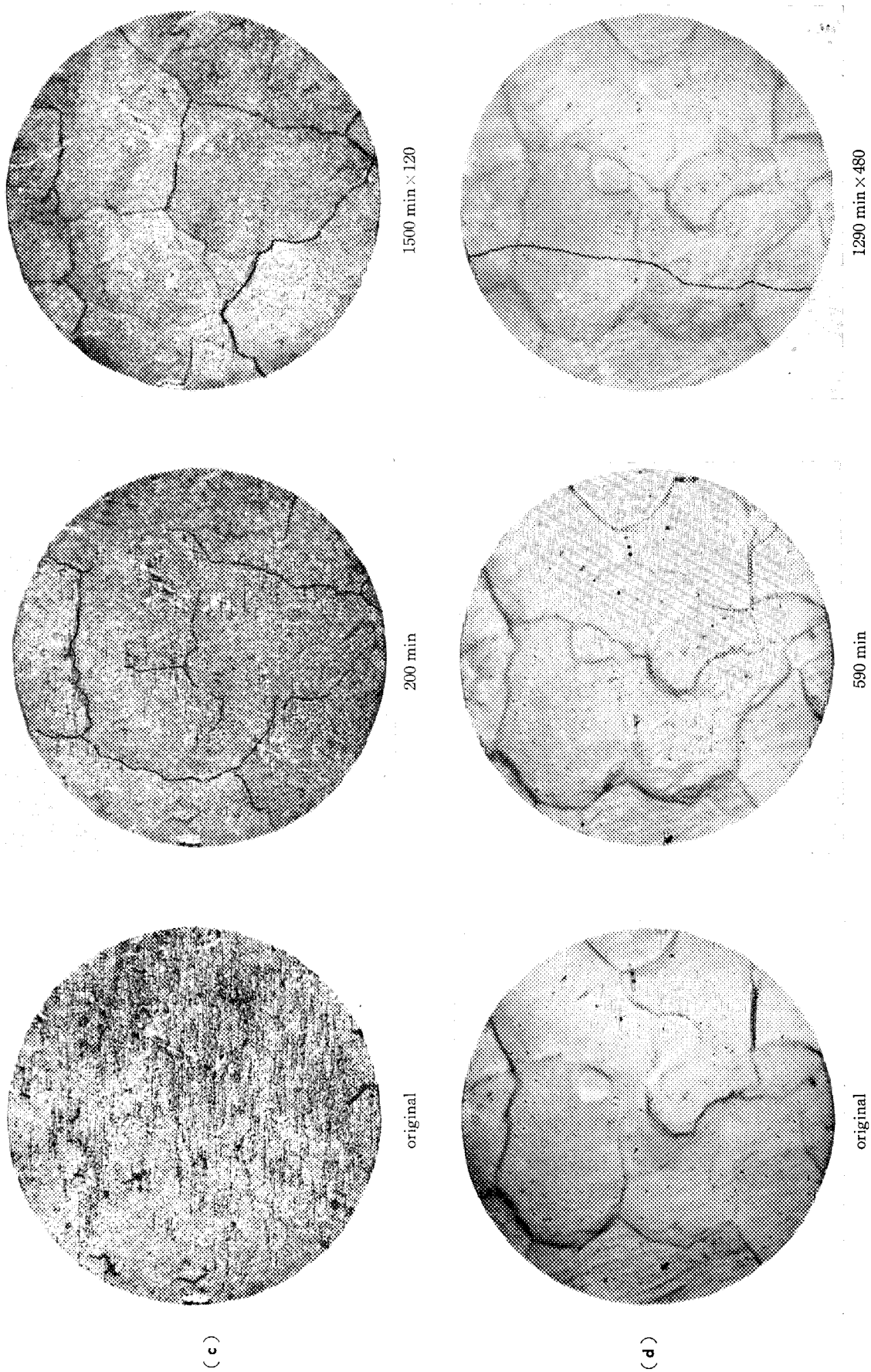


**Fig. 4** Observation of crack formation of oxide surface (700°C, in $O_2$).
(a) Unalloyed Zr No. 1, (b) Zr-2 w/o Cu, (c) Zr-2.5 w/o Nb, (d) Zircaloy-2

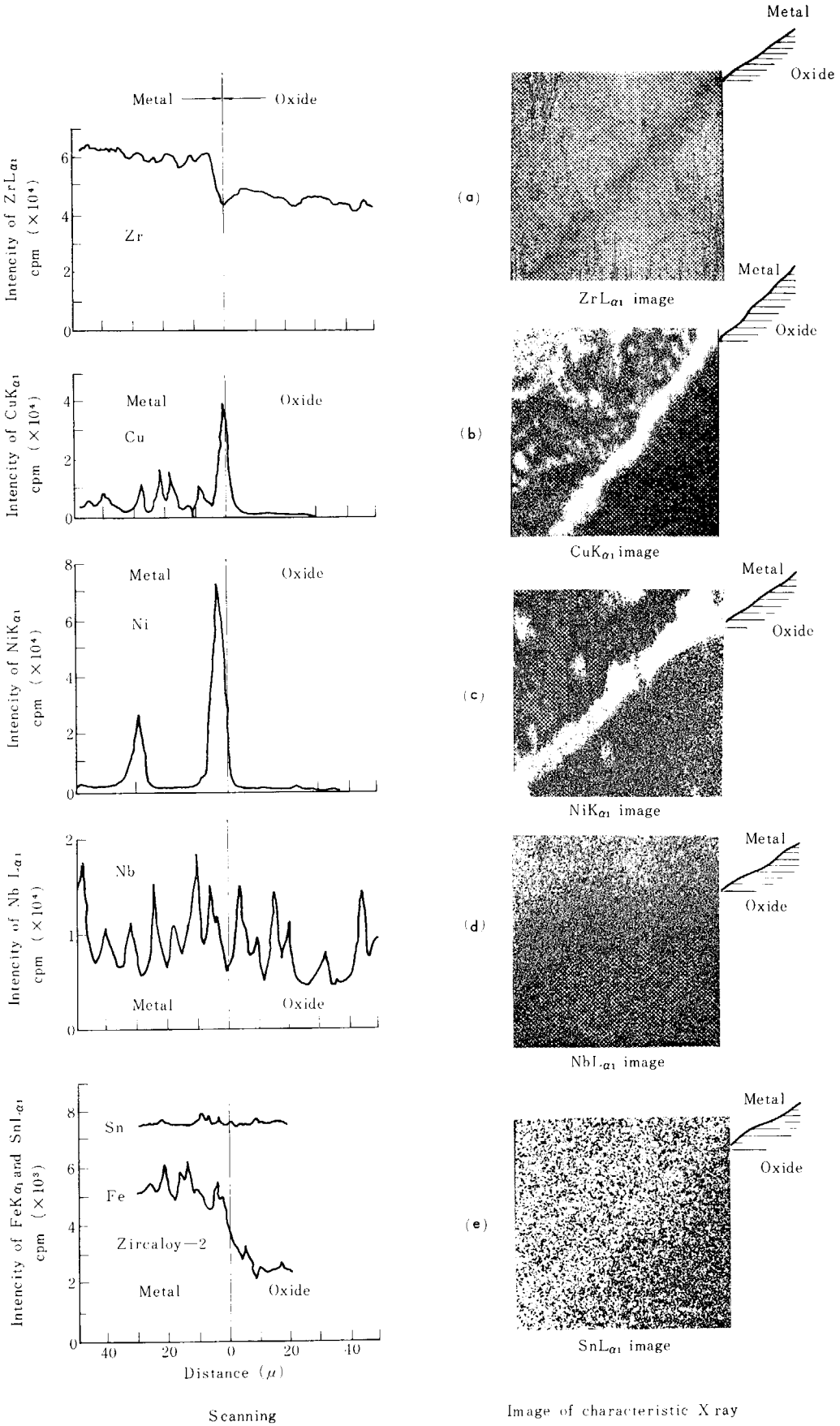


**Fig. 5** Charactaristic X-ray graphs and images of cross section of oxidized alloys.

(a) (b) Zr-2 wt/o Cu at 700°C, 4500 min (c) Zr-2 wt/o Ni at 700°C, 4300 min
(d) Zr-2.5 wt/o Nb at 700°C, 1500 min (e) Zry-2 as 800°C, 1000 min

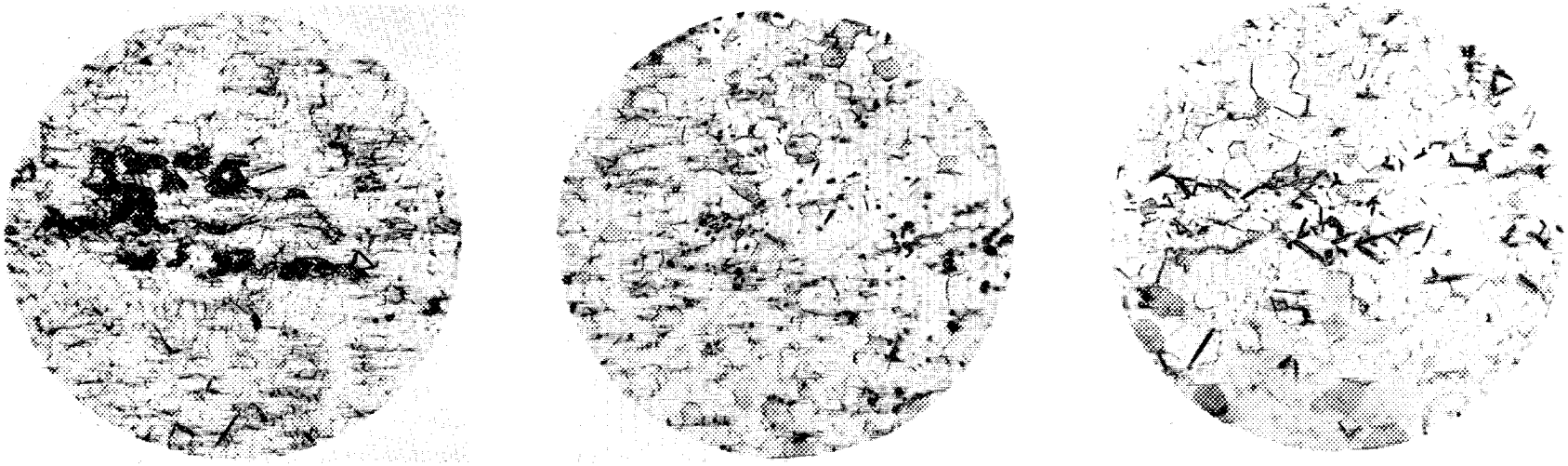

Unalloyed Zr No. 3　　Unalloyed Zr No. 2　　Unalloyed Zr No. 1　　×48

**Fig. 7** Microstructure of unalloyed zirconium. (etching solution ; 1 % HF + 1 % $HNO_3$ + 98% $H_2O$, 10 sec)